BIOCHEMISTRY
including biophysical chemistry & molecular biology

Article

pubs.acs.org/biochemistry

The Extent of Pyrene Excimer Fluorescence Emission Is a Reflector of Distance and Flexibility: Analysis of the Segment Linking the LDL Receptor-Binding and Tetramerization Domains of Apolipoprotein E3

Gursharan K. Bains, Sea H. Kim, Eric J. Sorin, and Vasanthy Narayanaswami*

Department of Chemistry and Biochemistry, 1250 Bellflower Boulevard, California State University Long Beach, Long Beach, California 90840, United States

ABSTRACT: Pyrene is a spatially sensitive probe that displays an ensemble of monomeric fluorescence emission peaks (375−405 nm) and an additional band (called excimer) at ∼460 nm when two fluorophores are spatially proximal. We examined if there is a correlation between distance between two pyrenes on an α-helical structure and excimer/monomer (e/m) ratio. Using structure-guided design, pyrene maleimide was attached to pairs of Cys residues separated by ∼5 Å increments on helix 2 of the N-terminal domain of apolipoprotein E3 (apoE3). Fluorescence spectral analysis revealed an intense excimer band when the probes were ∼5 Å from each other with an e/m ratio of ∼3.0, which decreased to ∼1.0 at 20 Å. An inverse correlation between e/m ratio and the distance between pyrenes was observed, with the probe and helix flexibility also contributing to the extent of excimer formation. We verified this approach by estimating the distance between T57C and C112 (located on helices 2 and 3, respectively) to be 5.2 Å (4.9 Å from NMR and 5.7 Å from the X-ray structure). Excimer formation was also noted to a significant extent with probes located in the linker segment, suggesting spatial proximity (10−15 Å) to corresponding sites on neighboring molecules in the tetrameric configuration of apoE. We infer that oligomerization via the C-terminal domain juxtaposes the linker segments from neighboring apoE molecules. This study offers new insights into the conformation of tetrameric apoE and presents the use of pyrene as a powerful probe for studying protein spatial organization.

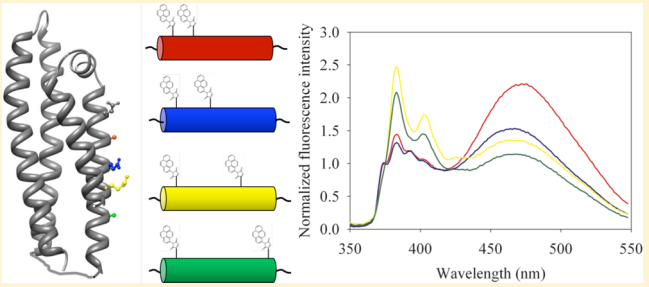

Pyrene is a molecular spectroscopic probe that has been used to study a wide range of biomolecules, including proteins, lipids, nucleic acids, and biomembranes. Its distinctive spectral features are exploited to obtain information regarding protein structure, molecular organization, and conformation. Site-specific labeling of proteins is typically achieved by conjugating pyrene with Cys or Lys,[1−4] using the reactivity of maleimide and iodoacetamide groups for the former, and those of succinimidyl ester, isothiocyanate, and sulfonyl chloride groups for the latter.[5] A major advantage of using pyrene for protein conformational analysis is its high extinction coefficient.[5] Pyrene-labeled proteins can thus be analyzed at very low (5−10 μg/mL), physiologically relevant protein concentrations. An added desirable feature of pyrene is its emission of fluorescence only upon covalent attachment to thiols. The double bond of the maleimide group significantly reduces the fluorescence emission and quantum yield of the unreacted fluorophore. Addition of the thiol group across the double bond of the maleimide group leads to a thioether linkage and significantly enhances the quantum yield.

The fluorescence emission spectrum of pyrene is characterized by an ensemble of five major vibronic bands designated bands I−V, with well-defined peaks at ∼375, 379, 385, 395, and 410 nm, respectively. These are attributed to the $\pi \rightarrow \pi^*$ transitions and are cumulatively termed the monomeric emission. The peak at 375 nm corresponds to the first vibronic band with a 0−0 transition, while that at 385 nm is attributed to the third vibronic band with a 0−2 transition.[6−8] Because the electronic and vibronic states are coupled,[6−8] band III is exquisitely sensitive to the polarity of the probe's microenvironment. It shows increased fluorescence emission intensity in comparison to that of band I in hydrophobic environments. In contrast, the intensity of band I will be higher than that of band III in polar environments.[9,10] In addition to the monomeric peaks, a broad, unstructured band appears at longer wavelengths (ranging from 425 to 550 nm, centered around 460 nm) when a ground state and an excited state pyrene ring are ∼10 Å from each other; they interact, giving rise to the excited state dimer or "excimer" emission.[11,12] The unusually long lifetime of pyrene emission (50−90 ns)[10,13] allows this excited state reaction to occur. Excimer emission may arise in a dose-dependent manner: for example at high concentration of pyrene-labeled proteins in solution, corre-

Received: April 24, 2012
Revised: July 5, 2012
Published: July 10, 2012

dx.doi.org/10.1021/bi3005285 | *Biochemistry* 2012, 51, 6207−6219

sponding to intermolecular interactions, or in the context of the plane of a lipid bilayer.[13]

The photophysics behind pyrene fluorescence is a complex phenomenon involving multiple species and processes.[11,14−16] Excitation of a ground state monomer (M) gives rise to an excited state monomer (M*), the decay of which results in a typical monomer emission spectrum between 375 and 410 nm. When M interacts with a spatially proximal M* to yield M·M* in a precise configuration, it leads to excimer (E*) formation, which is manifest as an excimer emission peak. It is also possible that the two interacting pyrenes are not in a favorable configuration for excimer formation, in which case a nonfluorescent complex may be formed. Whether two proximal pyrenes lead to excimer formation or a nonfluorescent complex appears to be determined by the local microenvironment.

Pyrene excimer fluorescence has been employed to study intra- and intermolecular interactions and spatial relationships in proteins.[17] We employ this technique to understand conformational organization in exchangeable apolipoproteins, a class of lipid-binding proteins that are predominantly α-helical in structure. Apolipoproteins possess an inherent structural adaptability that allows them to exist in lipid-free and lipoprotein-bound (or lipid-bound) states. We previously showed that apolipophorin III (apoLp-III) from the Sphinx moth *Manduca sexta*, a five-helix bundle protein, undergoes a dramatic lipid-triggered conformational change, involving opening of the helix bundle, which allows interaction of the hydrophobic side of the amphipathic α-helices with the lipid surface.[18] Helix bundle opening was demonstrated using a disulfide bonding-mediated "locking" strategy involving targeted amino acid substitution with pairs of substituted Cys residues (N40C/L90C and A8C/A138C), which lead to a loss of function.[19−21] It was confirmed by pyrene fluorescence studies, which revealed modest excimer formation between probes located on the N40C/L90C or A8C/A138C pairs in the helix bundle state that decreased significantly upon lipid interaction. The data were interpreted as N40C/L90C (and A8C/A138C) Cys pairs being located ∼10 Å from each other in the lipid-free state and >10 Å from each other in the lipid-bound state. Subsequent NMR studies revealed distances of 13 Å between the Cα atoms of N40 and L90 and 9.5 Å between A8 and A138 in lipid-free apoLp-III.[22] A recent report from our group on the isolated apoE CT domain (residues 201−299)[23] employed site-specific labeling of singly Cys-substituted variants (at positions 223, 255, and 277) with pyrene, which revealed dominant excimer bands. This suggested intermolecular spatial proximity (∼10 Å) due to apoE self-association mediated by helix−helix interactions between neighboring apoE molecules. In all of these studies, the mere appearance of the excimer band was interpreted as the specified sites lying within 10 Å of each other, regardless of the extent of excimer intensity (relative to the monomer intensity at 375 nm) or excimer/monomer (e/m) ratio.[17]

In this study, we investigated if there is a correlation between the distance between two pyrene-bearing locations and the extent of pyrene excimer fluorescence, or e/m ratio. Pyrene maleimide was attached to pairs of Cys residues on an α-helical structure as a "scaffold", followed by analysis of excimer formation by fluorescence spectroscopy (Figure 1A). The α-helix that was selected as the scaffold was helix 2 of the apoE3 NT domain encompassing residues 1−191. We employed a structure-guided design to place the pyrenes on Cys substituted at defined distances based on the available high-resolution

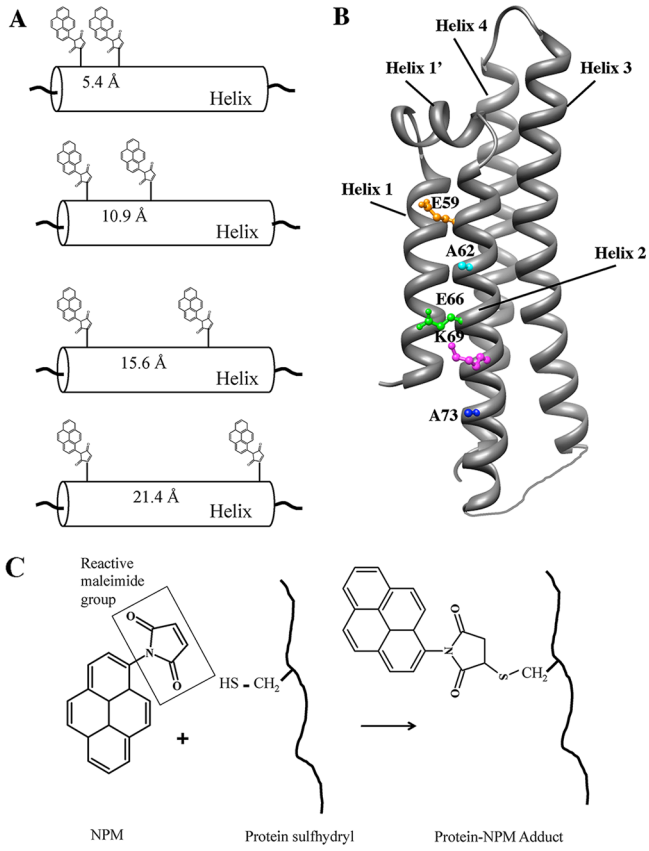

Figure 1. Design of single- and double-Cys constructs in helix 2 of apoE(1−191) for site-directed labeling. (A) Schematic representation of the placement of pyrene rings along a helix. (B) Sites selected for substitution with a Cys in helix 2 of apoE3(1−191) based on the X-ray structure of apoE3(1−191)[24] (PDB entry 1NFN). The distances between the Cα atoms of pairs of residues are listed in Table 2. (C) Reaction between the sulfhydryl group of Cys and NPM.

structure of apoE3(1−191).[24,25] We validated our observation of the correlation between distance and e/m ratio from the X-ray structure by determining the spatial proximity between sites located on two different helices within the NT domain. Lastly, we applied this approach to define the spatial organization of a portion of the loop segment linking the NT and CT domains among neighboring molecules in the native lipid-free tetrameric state of full-length apoE3.

MATERIALS AND METHODS

Materials. *N*-(1-Pyrene)maleimide (NPM) was obtained from Invitrogen (Molecular Probes, Eugene, OR), dithiothreitol (DTT, 99% pure) from Acros Organics (Morris Plains, NJ), guanidine hydrochloride (GdnHCl, 99% pure) from Fisher Scientific (Fair Lawn, NJ), 2,2,2-trifluoroethanol (TFE) from Sigma Aldrich (St. Louis, MO), and glycerol from Calbiochem EMD Biosciences, Inc. (La Jolla, CA). All solvents used were of analytical grade.

Design of Cys Constructs. Single- and double-Cys constructs were designed by examining the X-ray crystal structure of apoE3(1−191) (PDB entry 1NFN) using the freely available online Chimera software developed by UCSF (Table 1). The presence of Cys residues allows us to covalently attach fluorophores using sulfhydryl-reactive functional groups. The pairs of residues that were selected for substitution with Cys were E59 and A62, E59 and E66, E59 and K69, and E59 and

dx.doi.org/10.1021/bi3005285 | *Biochemistry* 2012, 51, 6207−6219

Table 1. Single- and Double-Cys apoE Constructs

apoE(1−191) constructs
apoEC112S/E59C(1−191)
apoEC112S/A62C(1−191)
apoEC112S/E66C(1−191)
apoEC112S/K69C(1−191)
apoEC112S/A73C(1−191)
apoEC112S/E59C/A62C(1−191)
apoEC112S/E59C/E66C(1−191)
apoEC112S/E59C/K69C(1−191)
apoEC112S/E59C/A73C(1−191)
apoEC112S/V161C(1−191)[a]
apoEC112S/G169C(1−191)[a]
apoEC112S/A176C(1−191)[a]
apoEC112S/L181C(1−191)[a]
apoE(1−299) constructs
apoEC112S/V161C(1−299)[a]
apoEC112S/G169C(1−299)[a]
apoEC112S/A176C(1−299)[a]
apoEC112S/L181C(1−299)[a]
controls
apoE3(1−191)
apoE3T57C(1−191)
apoEC112S(1−191)
apoE3(1−299)
apoEC112S(1−299)

[a]Available from ref 26.

A73 (Figure 1B). In addition, single-Cys substitutions were introduced at the following sites: E59, A62, E66, K69, and A73.

Site-Directed Mutagenesis. Primers were designed using an online tool (http://www.chem.agilent.com) and were synthesized by Eurofins MWG OPERON (Huntsville, AL). Wild-type (WT) apoE3(1−191) bears a single endogenous Cys at position 112; this was first replaced with serine (with no significant change in function or fold), and the construct was designated apoEC112S(1−191) as described previously[26] (throughout this work, constructs with Ser at position 112 instead of Cys are simply termed apoE, not apoE3). Subsequently, single-Cys constructs E59C, A62C, E66C, K69C, and A73C and double-Cys constructs E59C/A62C, E59C/E66C, E59C/K69C, and E59C/A73C were generated in apoEC112S(1−191)/pET20b using the QuikChange II Site Directed Mutagenesis Kit (Agilent Technology, Stratagene, La Jolla, CA). In addition, a double-Cys construct, apoE3T57C(1−191), was generated for the purpose of validation. Lastly, a set of apoEC112S(1−191) and apoEC112S(1−299) constructs with a single Cys probing the segment from position 161 to 181[26] at four different locations were utilized to assess the intermolecular spatial organization of the native tetrameric protein. The plasmids were sequenced at the DNA sequencing facility of the University of California (Berkeley, CA) to confirm the presence of the desired mutations using CLC Sequence Viewer. All the constructs employed in this study are listed in Table 1. The controls used throughout the study include apoE3(1−191), apoEC112S(1−191), apoE3(1−299), and apoEC112S(1−299).

Expression, Isolation, and Purification of apoE Constructs. The pET22b expression vector bears ampicillin resistance and encodes WT, single-Cys, or double-Cys apoE, with a hexahistidine tag at the N-terminal end. The recombinant proteins were overexpressed in *Escherichia coli* as described previously.[23] Following expression, the resuspended cells were lysed using a microfluidizer (Microfluidics, Newton, MA) and the recombinant proteins were purified using a Ni^{2+} affinity matrix (Hi-Trap chelating column, GE Healthcare, Piscataway, NJ). Protein purity was verified by sodium dodecyl sulfate−polyacrylamide gel electrophoresis (SDS−PAGE) analysis using a 4 to 20% acrylamide gradient under reducing and nonreducing conditions. The protein concentration was determined in a Nano-Drop 2000/2000c spectrometer (Thermo Fisher Scientific, Wilmington, DE) using molar extinction coefficients at 280 nm of 27960 and 44460 M^{-1} cm^{-1} for apoE3(1−191) and apoE3(1−299), respectively.

Circular Dichroism (CD) Spectroscopy. CD measurements were performed on a Jasco 810 spectropolarimeter at 24 °C. Far-UV CD scans were recorded between 185 and 260 nm in 10 mM sodium phosphate buffer (pH 7.4) using protein concentrations of 0.2 mg/mL in a 0.1 cm path length cuvette. When CD scans of unlabeled protein were recorded, the sample was preincubated with a 5-fold molar excess of DTT for 4 h at 37 °C prior to measurements to reduce intermolecular disulfide bonds. The CD profiles were the average of four independent scans, with a response time of 2 s and a bandwidth of 1 nm. The molar ellipticity ($[\theta]$) in degrees square centimeter per decimole at 222 nm was obtained using the equation

$$[\theta]_{222} = (\mathrm{MRW} \times \theta)/(10lc)$$

where MRW is the mean residue weight (obtained by dividing the molecular weight by the number of residues), calculated to be 115.7 for apoE3(1−191) and 114.4 for apoE3(1−299); θ is the measured ellipticity in degrees at 222 nm; l is the cuvette path length (in centimeters); and c is the protein concentration (in grams per milliliter). The percent α-helix content was calculated as described previously:[27]

$$\%\,\alpha\text{-helix} = 100\% \times (3000 - [\theta]_{222})/39000$$

GdnHCl-Induced Unfolding. Unfolding of apoE(1−191) variants (0.2 mg/mL) was assessed by following changes in molar ellipticity at 222 nm as a function of increasing concentrations of GdnHCl. The samples were treated with GdnHCl in the presence of 0.5 mM DTT in 10 mM sodium phosphate buffer (pH 7.4) for 18 h at 24 °C. The percent maximal change was calculated from the ellipticity values at 222 nm as described previously,[23] and the concentration of GdnHCl required to cause a 50% decrease in the maximal change was calculated for each construct.

Labeling with NPM. Single- and double-Cys apoE variants [3 mg of protein in 10 mM ammonium bicarbonate (pH 7.4)] were initially preincubated with a 5-fold molar excess of DTT and 2 M GdnHCl for 4 h at 37 °C to reduce inter- and/or intramolecular disulfide bonds. This was followed by incubation with a 10-fold molar excess (over apoE) of NPM (dissolved in DMSO) for 16 h at 37 °C. NPM that precipitated during the incubation was removed by centrifugation at 13000*g* for 10 min. The labeled samples were passed through a 1 mL Ni^{2+} affinity Hi-Trap chelating column to remove excess DTT, GdnHCl, and NPM. All purified pyrene-labeled proteins were dialyzed against 10 mM sodium phosphate (pH 7.4) and 150 mM NaCl [phosphate-buffered saline (PBS)] for 48 h at 4 °C with three buffer changes. The stoichiometry of labeling was calculated using the absorbance of the protein at 280 nm and pyrene at 345 nm (molar extinction coefficient of pyrene at 345 nm in methanol, 40000 M^{-1} cm^{-1}).

dx.doi.org/10.1021/bi3005285 | *Biochemistry* 2012, 51, 6207−6219

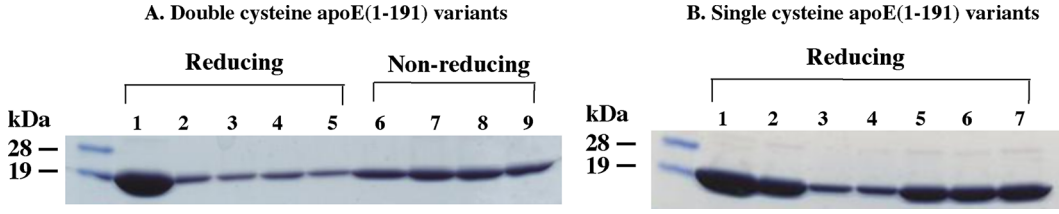

Figure 2. SDS−PAGE analysis of single- and double-Cys apoE(1−191) variants. (A) SDS−PAGE analysis (4 to 20% acrylamide gradient) of purified apoE(1−191) double-Cys variants conducted under reducing (lanes 2−5) and nonreducing (lanes 6−9) conditions. The lane assignments following molecular mass standards are as follows: lane 1, apoE3(1−191); lanes 2 and 6, apoEC112S/E59C/A62C; lanes 3 and 7, apoEC112S/E59C/E66C; lanes 4 and 8, apoEC112S/E59C/K69C; lanes 5 and 9, apoEC112S/E59C/A73C. (B) Electrophoresis of single-Cys apoE(1−191) variants conducted under reducing conditions. The lane assignments following molecular mass standards are as follows: lane 1, apoE3(1−191); lane 2, apoEC112S(1−191); lane 3, apoEC112S/E59C(1−191); lane 4, apoEC112S/A62C(1−191); lane 5, apoEC112S/E66C(1−191); lane 6, apoEC112S/K69C(1−191); lane 7, apoEC112S/A73C(1−191).

Gel Filtration Chromatography. Gel filtration chromatography of singly labeled variants apoEC112S/E59C(1−191) and apoEC112S/A62C(1−191) was conducted on a 80 mL column packed with Sepharose CL-6B (Sigma Aldrich, St. Louis, MO) with a flow rate of 0.75 mL/min in PBS. In addition, human serum albumin, apoEC112S(1−191), and *Locusta migratoria* apolipophorin-III (molecular masses of 66400, 24017, and 17398 Da, respectively) were used as controls to estimate the molecular mass and self-associated state of the labeled variants. The fractions (2 mL) were monitored at 280 nm.

Fluorescence Measurements. Steady state fluorescence analyses were performed on a Perkin-Elmer LS55B fluorometer at 24 °C. Fluorescence emission spectra of pyrene-labeled samples (5−10 μg/mL) were recorded in PBS between 350 and 550 nm by setting the excitation wavelength at 345 nm. The excitation and emission slit widths were set at 5 nm. The scan speed was 50 nm/min; an average of 10−20 scans was recorded. In select experiments, the samples were either diluted with PBS or treated with increasing concentrations of TFE or glycerol [0−50% (v/v)] prior to the spectra being recorded.

RESULTS

To determine if there is a correlation between the extent of pyrene excimer fluorescence and distance between two pyrene-bearing locations on an α-helix, pairs of residues were selected for substitution with Cys, starting from E59: E59 and A62, E59 and E66, E59 and K69, and E59 and A73 (Figure 1B). The selected sites were polar in nature and faced away from the helix bundle interior. The distances between the Cα atoms of the selected pairs were 5.4, 10.9, 15.6, and 21.6 Å, respectively.

The single- and double-cysteine apoE variants bearing a hexahistidine tag at the N-terminal end were overexpressed in *E. coli*, isolated, and purified as described previously.[23] Briefly, the recombinant proteins were purified using a Ni^{2+} affinity matrix, dialyzed against 20 mM ammonium bicarbonate (pH 7.4), lyophilized, and stored at −20 °C until further use. Figure 2A shows the SDS−PAGE analysis of the double-Cys variants that were used under reducing and nonreducing conditions. Single-Cys variants were generated as controls (Figure 2B). A 22 kDa band was noted in all cases of apoE(1−191) and a 34 kDa band for all apoE(1−299) variants (data not shown) under reducing conditions. The proteins were used without further purification; they were preincubated with DTT under denaturing conditions (in the presence of GdnHCl) prior to being labeled, to ensure reduction of intra- or intermolecular disulfide bonds that may have arisen during isolation and purification. Standard maleimide chemistry[5] was used to covalently attach the pyrene to Cys as described by us previously[23] (Figure 1C). The stoichiometry of labeling was found to be 0.5 and 1.5 for single- and double-Cys apoE, respectively. The likelihood that pyrene is attached non-covalently to hydrophobic sites is very low because the labeling was conducted in the presence of 2 M GdnHCl followed by extensive washing in the presence of denaturant on the Ni^{2+} affinity column. The labeled proteins were refolded by extensive dialysis against PBS.

CD analysis was performed on all the variants in their reduced state to verify their secondary structure (Figure 3). In general, most variants adopt an α-helical structure with α-helical contents of 41−48%. apoEC112S/E59C/E66C(1−191) was an exception with an α-helical content of ∼30%. Stability studies indicated that the midpoint of GdnHCl-induced unfolding was ∼2.5 M for each double- and single-Cys construct. This suggests that the global fold is broadly similar to that of WT apoE3(1−191).[28]

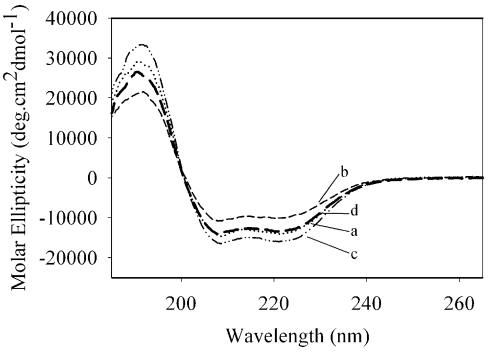

Figure 3. Far-UV CD spectra of apoE(1−191) constructs. Far-UV CD spectra of (a) apoEC112S/E59C/A62C(1−191), (b) apoEC112S/E59C/E66C(1−191), (c) apoEC112S/E59C/K69C(1−191), and (d) apoEC112S/E59C/A73C(1−191) (0.2 mg/mL) in the presence of DTT. Spectra were recorded from 185 to 260 nm in 10 mM sodium phosphate (pH 7.4). An average of four scans was recorded, using a 0.1 cm path length cell, a scan speed of 50 nm/min, and a response time of 2 s.

Figure 4A shows the fluorescence emission spectra of pyrene-labeled double-Cys apoE(1−191) variants in PBS (5 μg/mL) bearing probes at positions 59 and 62 (a), 59 and 66 (b), 59 and 69 (c), or 59 and 73 (d). The peaks at ∼375 and 385 nm are designated as bands I and III, respectively. Each spectrum was normalized with respect to the fluorescence emission intensity of the first monomer peak at 375 nm. The two

dx.doi.org/10.1021/bi3005285 | *Biochemistry* 2012, 51, 6207−6219

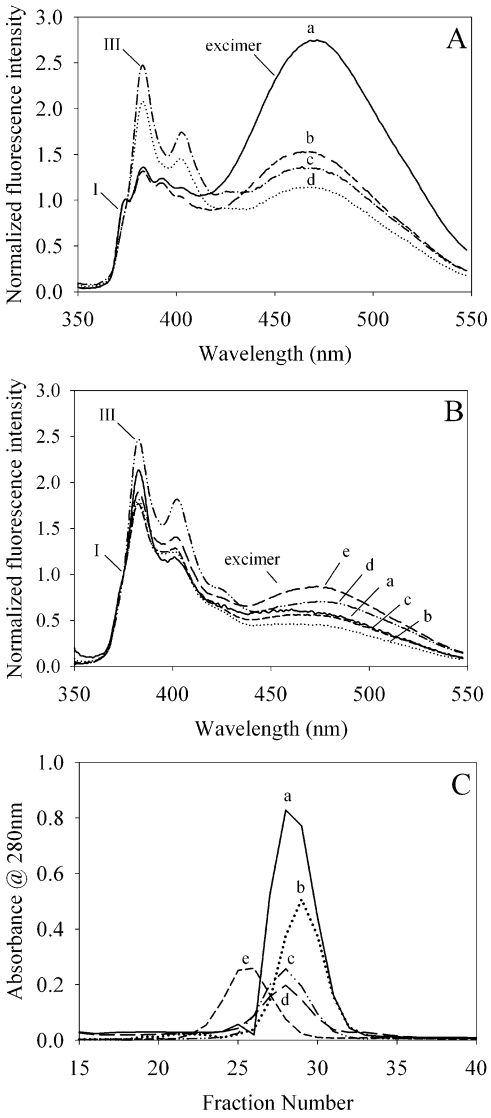

Figure 4. Fluorescence emission spectra of pyrene-labeled double- and single-Cys apoE NT variants. Fluorescence emission spectra of pyrene-labeled proteins (5 μg/mL) were recorded in PBS. (A) Double-Cys variants: (a) apoEC112S/E59C/A62C(1−191), (b) apoEC112S/E59C/E66C(1−191), (c) apoEC112S/E59C/K69C(1−191), and (d) apoEC112S/E59C/A73C(1−191). (B) Single-Cys variants: (a) apoEC112S/E59C(1−191), (b) apoEC112S/A62C(1−191), (c) apoEC112S/E66C(1−191), (d) apoEC112S/K69C(1−191), and (e) apoEC112S/A73C(1−191). The spectra were normalized to the peak at 375 nm. Bands I and III and the excimer bands are indicated. All spectra shown are average of 10 scans (recorded at a scan speed of 50 nm/min) with the excitation wavelength set at 345 nm (excitation and emission slit widths set at 5 nm). (C) Gel filtration chromatography of pyrene-labeled single-Cys variants: (a) apoEC112S(1−191) (24 kDa), (b) apoLp-III (18 kDa), (c) pyrene-labeled apoEC112S/E59C(1−191), (d) pyrene-labeled apoEC112S/A62C(1−191), and (e) monomeric human serum albumin (~66 kDa).

variants in which the pyrenes are farthest apart, i.e., at positions 59 and 69 and positions 59 and 73, spectra c and d, respectively, display a significantly higher intensity for band III than for band I, indicative of a relatively hydrophobic microenvironment for these pyrene pairs.

In addition to the monomeric family of bands, a significant excimer band centered ~460 nm was noted for each doubly labeled variant. However, the intensity of the excimer band varied depending on the distance between the pyrenes. To compare the relative intensities between the variants, the *e*/*m* ratio was calculated by comparing the fluorescence intensity of the excimer band at 460 nm to the first monomer peak at 375 nm (Table 2). The probes located at positions 59 and 62 displayed the highest excimer emission intensity, followed in order by those at positions 59 and 66, 59 and 69, and 59 and 73 (*e*/*m* ratios of 2.6, 1.5, 1.4, and 1.2, respectively). For comparison, the spectra of pyrene-labeled single-Cys variants in each of these positions are shown in Figure 4B. A significantly lower extent of excimer formation is noted in all cases of pyrene-labeled single-Cys variants, with *e*/*m* ratios varying between 1.0 and 0.5 (band I appears as a shoulder). To check the possibility that pyrene labeling promotes self-association of the singly labeled proteins, gel filtration chromatography was conducted; the profiles of pyrene-labeled apoEC112S/E59C(1−191) and apoEC112S/A62C(1−191) are shown as examples (Figure 4C). The molecular masses of the singly labeled variants were found to be ~24 kDa, corresponding to that of monomeric apoEC112S(1−191); the Cys-less variant was used to ensure that there are no disulfide-linked dimers in the sample. This confirms that the presence of pyrene does not promote self-association of the variant.

To investigate the possibility that the excimer band in the double-Cys variants arises because of intermolecular spatial proximity between pyrenes on neighboring molecules, a 50 μg/mL solution of each doubly labeled variant was diluted 1.25-, 2.5-, and 10-fold with PBS. As expected, the spectra revealed decreases in monomer emission intensities in each case; however, the decrease in the *e*/*m* ratio was not congruent with the dilution factor. This is illustrated using the examples of pyrene-labeled apoEC112S/E59C/A62C(1−191) and apoEC112S/E59C/K69C(1−191) (Figure 5A,B), where each spectrum was multiplied by the dilution factor and normalized with respect to the emission intensity at 375 nm. The observation that the *e*/*m* ratio does not decrease with the dilution factor indicates that the excimer emission is predominantly due to intramolecular proximity. The contribution of intermolecular spatial proximity of two pyrenes to excimer formation appears to be a minor factor. Other pyrene-labeled double-Cys variants (positions 59 and 66 and positions 59 and 73) show a similar trend upon dilution (data not shown).

In an independent approach, the possibility of the contribution of intermolecular interactions to excimer formation was examined by monitoring the effect of disrupting quaternary interactions. This was accomplished by monitoring the effect of TFE on the fluorescence emission characteristics of all the double-Cys-labeled variants. TFE increased the α-helical content of all the variants by a similar extent (data not shown). The effects of 50% TFE on the fluorescence emission spectra of pyrene-labeled apoEC112S/E59C/A62C(1−191) and apoEC112S/E59C/K69C(1−191) are shown as examples (panels A and B of Figure 6, respectively). The effect of TFE is manifested as three key spectral features: (i) no significant change in the *e*/*m* ratio (Table 2), (ii) a minor red shift in the wavelength of maximal fluorescence emission for the excimer band, and (iii) a decrease in the intensity of band III accompanied by the appearance of a distinct band I peak. Other pyrene-labeled double-Cys variants (positions 59 and 66 and positions 59 and 73) display a similar trend in their response to increasing TFE concentrations (data not shown).

dx.doi.org/10.1021/bi3005285 | *Biochemistry* 2012, 51, 6207−6219

Table 2. *e*/*m* Ratios for Pyrene-Labeled Double-Cys apoE(1−191) Variants

		distance (Å) (NMR[b,c])			*e*/*m* ratio		
Cα positions	distance (Å) (X-ray[a])	apoE(1−183)	apoE(1−299)	pyrene-labeled apoE(1−191) variant	buffer[d]	50% glycerol[d]	50% TFE[d]
E59 and A62	5.4	5.3	5.0	E59C/A62C	2.62 ± 0.25	1.12 ± 0.02	1.83 ± 0.06
E59 and E66	10.9	10.9	10.8	E59C/E66C	1.50 ± 0.01	0.91 ± 0.02	1.20 ± 0.01
E59 and K69	15.6	15.3	15.3	E59C/K69C	1.40 ± 0.06	0.78 ± 0.01	0.99 ± 0.04
E59 and A73	21.6	21.1	21.2	E59C/A73C	1.22 ± 0.12	0.68 ± 0.04	0.90 ± 0.04

[a]From ref 24. [b]From ref 25. [c]From ref 65. [d]Protein concentration of 5 μg/mL.

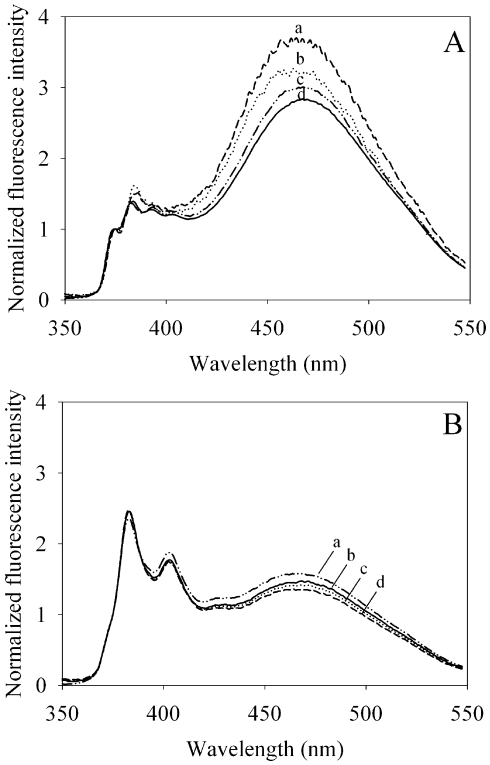

Figure 5. Effect of dilution on pyrene excimer fluorescence. The effect of dilution on the fluorescence emission spectra of pyrene-labeled double Cys variants is shown for (A) apoEC112S/E59C/A62C(1−191) and (B) apoEC112S/E59C/K69C(1−191). The spectra were recorded at 50, 40, 20, and 5 μg/mL (a−d, respectively). Spectral measurements were taken as described in the legend of Figure 4. Each spectrum was multiplied by the dilution factor and normalized to the peak at 375 nm to illustrate the effect of dilution on the *e*/*m* ratio.

Taken together, we conclude that the excimer noted is predominantly due to intramolecular spatial proximity between probes located along a single helix.

In the next step, the contribution of probe flexibility to the extent of excimer formation was studied. This was accomplished by monitoring the effect of altering the viscosity of the medium on fluorescence emission characteristics of the labeled variants. The rationale is that increasing the viscosity of the medium may decrease the mobility of the fluorophores and therefore the chance of two pyrene rings encountering each other during the lifetime of its excited state; if this were the case, we would predict that the excimer formation or intensity would decrease progressively with an increasing viscosity. The viscosity of the buffer was varied (1.005, 1.31, 1.76, 2.5, 3.72, and 6.0 mPa/s at 20 °C) by using increasing amounts of glycerol (0, 10, 20, 30, 40, and 50%, respectively). Figure 6C shows the effect of 0−50% (v/v) glycerol on the fluorescence emission of pyrene-labeled apoEC112S/E59C/A62C(1−191) as an example. A trend of a decrease in excimer formation and *e*/*m* ratio was noted with increasing glycerol concentrations. Other double-Cys variants (positions 59 and 66, 59 and 69, and 59 and 73) showed similar changes in the presence of varying amounts of glycerol (data not shown).

Figure 6D and Table 2 summarize the *e*/*m* ratios under different conditions. The following conclusions can be derived from these data. (i) There is an inverse correlation between *e*/*m* ratio and the distance between Cα atoms of two specified sites. (ii) The correlation is present even upon significant dilution, indicating that the excimer arises from intramolecular proximity. (iii) Upon disruption of the tertiary and quaternary interactions in the protein with TFE, this correlation is still observed, further confirming intramolecular interaction between pyrene rings. (iv) In the presence of glycerol, although the *e*/*m* ratios are lower, the correlation is still observed. To test the possibility of using this correlation to estimate the distance between sites, we generated an apoE(1−191) construct (bearing an endogenous Cys at position 112 in helix 3) with a Cys substituted at position 57 in lieu of Thr in helix 2.[29] In this intramolecular situation, the two pyrene rings are located on different helices; the distance between the Cα atoms of C112 and T57 was found to be 5.7 Å from the X-ray structure (PDB entry 1NFN) (Figure 7A) and 4.9 Å from the NMR structure (PDB entry 2KC3). The fluorescence emission spectrum of pyrene-labeled apoE3T57C(1−191) (Figure 7B) revealed a significant excimer band with an *e*/*m* ratio of 2.9, corresponding to a distance of 5.2 Å. For comparison, the spectrum of (singly) pyrene-labeled apoE3(1−191) is shown.

Lastly, we applied the correlation between the extent of pyrene excimer formation and distance to estimate intermolecular spatial proximity of a segment in the linker region (spanning residues 165−181) of apoE3 in its tetrameric configuration. Full-length apoE and apoE truncated at the C-terminal end up to position 191 were used, which allowed us to follow the effect of the presence of the CT domain (bearing apoE self-association sites) on the spatial organization of the linker segment. ApoE variants bearing a single Cys in the linker segment were examined (Table 1). Panels A and B of Figure 8 show the spectra of pyrene-labeled apoEC112S(1−299) and apoEC112S(1−191), respectively; the probes are at positions 161, 169, 176, and 181. Residue 161 (located at the C-terminal end of helix 4) was included as a control. Excimer formation was noted to a significant extent with apoEC112S(1−299) variants, with *e*/*m* ratios ranging from 2.0 to 1.2. The excimer was attributed to the intermolecular proximity between the individual subunits of tetrameric apoE. These ratios suggest that positions 161, 169, 176, and 181 are spatially proximal (8−15 Å) to the corresponding sites on neighboring molecules. Excimer bands were also noted for apoEC112S(1−191) variants, albeit to a lesser extent, with the *e*/*m* ratio ranging from 1.0 to 0.6, corresponding to intermolecular distances of 20−30 Å between these positions on neighboring molecules.

dx.doi.org/10.1021/bi3005285 | *Biochemistry* 2012, 51, 6207−6219

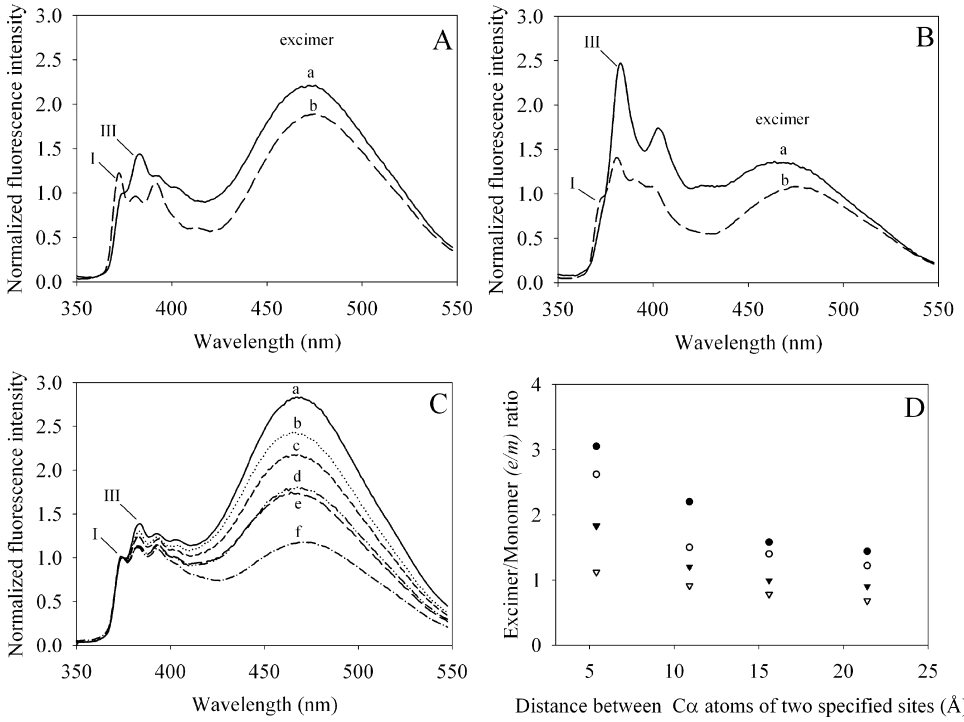

Figure 6. Effect of TFE and glycerol on pyrene excimer fluorescence. Fluorescence emission spectra of 5 μg/mL (A) pyrene-labeled apoEC112S/E59C/A62C(1−191) and (B) apoEC112S/E59C/K69C(1−191) were recorded in the presence of PBS (a) or 50% TFE (v/v) in PBS (b). Bands I and III are shown. (C) Fluorescence emission spectra of pyrene-labeled apoEC112S/E59C/A62C(1−191) were recorded in the presence of 0, 10, 20, 30, 40, and 50% (v/v) glycerol in PBS (a−f, respectively). Spectral measurements were taken as described in the legend of Figure 4. (D) Correlation between the extent of pyrene excimer formation and the distance between labeled sites. Plot of the *e*/*m* ratio vs the distance between the two C*α* sites bearing pyrene in 50 μg/mL PBS (●), 5 μg/mL PBS (○), 50% TFE (▼), and 50% glycerol (▽).

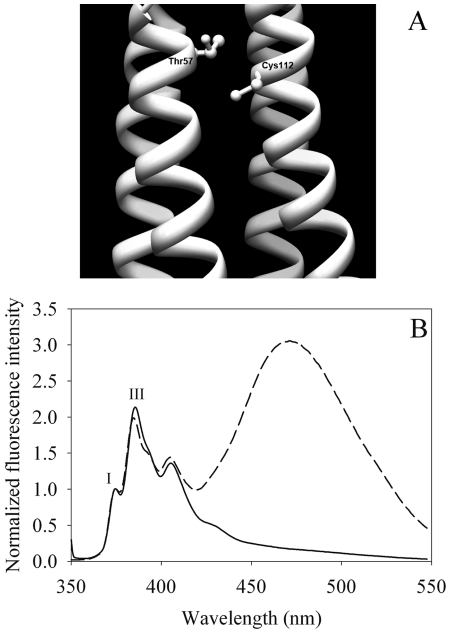

Figure 7. Estimation of the distance between positions 57 and 112 in apoE3 by pyrene excimer fluorescence analysis. (A) Close-up of the X-ray crystal structure of apoE3(1−191) (PDB entry 1NFN) showing the proximity between T57 and C112 (distance between the C*α* atoms of 5.7 Å). (B) Fluorescence emission spectra of pyrene-labeled apoE3T57C(1−191) (−−−) and apoE3(1−191) (—). From the plot shown in Figure 6D, the distance between positions 57 and 112 is estimated to be 5.2 Å.

Our studies indicate that interaction between the entire CT domain likely juxtaposes the linker segments from neighboring molecules, as evidenced by excimer formation. Truncation of residues 192−299 in apoE removes the principal sites responsible for facilitating intermolecular interactions. The effect of 50% TFE and 50% glycerol on the fluorescence emission features of pyrene-labeled variants was followed: apoEC112S/V161C(1−299) (Figure 8C) and apoEC112S/L181C(1−299) (Figure 8D) are shown as examples. In both variants, the excimer intensity was significantly lowered in the presence of TFE (*e*/*m* ratio from 1.6−2.0 to ∼0.2), because of dissociation of the tetramer. Glycerol also caused a decrease in excimer intensity to an *e*/*m* ratio of ∼1.0. Similar observations were noted for other linker variants (data not shown).

■ DISCUSSION

The photophysical processes governing the fluorescence emission of pyrene have been well characterized.[11,12,15] This has facilitated the extensive use of pyrene to monitor protein conformation and conformational changes . Typically, pyrene is attached covalently to a naturally occurring or substituted Cys residue(s) to probe a specified site(s). Pyrene excimer fluorescence emission has been exploited to obtain information about the conformation and molecular organization of several proteins,[30−33] including apolipoproteins.[19−21,23,34] In all these studies, a wide range of excimer emission intensities (relative to the intensity of band I of the monomeric ensemble) was noted and generally attributed to a distance of ∼10 Å between two probes. In this study, we investigated (i) the correlation between the distance between two pyrene-bearing locations and the extent of excimer fluorescence, (ii) the contribution of

dx.doi.org/10.1021/bi3005285 | *Biochemistry* 2012, 51, 6207−6219

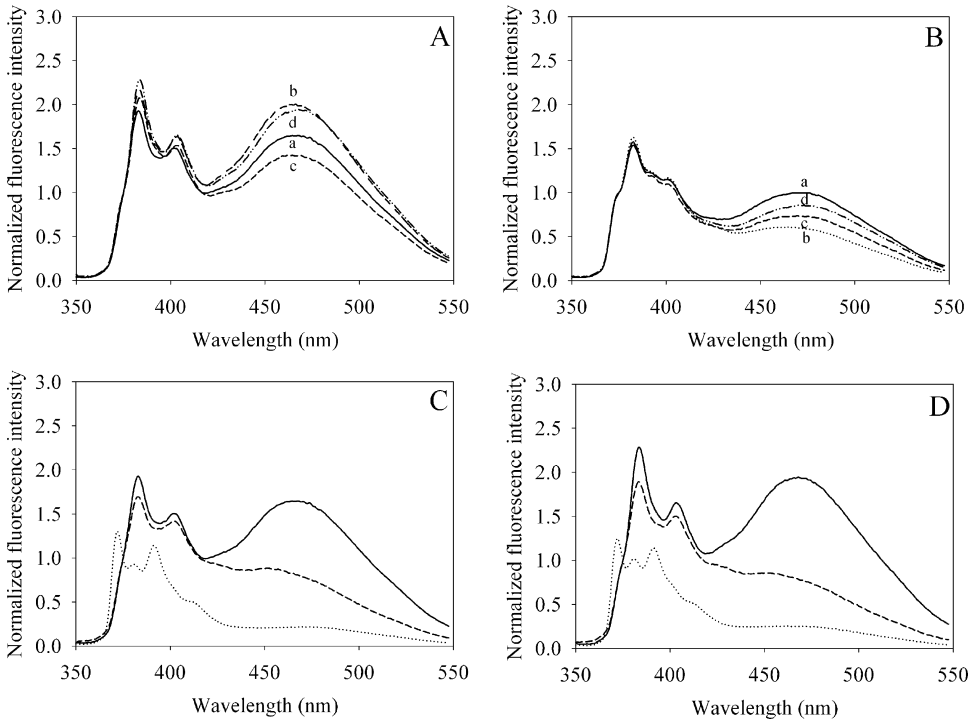

Figure 8. Fluorescence emission spectra of single-Cys apoE full-length and NT variants bearing pyrene in the linker segment. (A and B) Fluorescence emission spectra of (5 μg/mL) (A) apoEC112S(1−299) and (B) apoEC112S(1−191) bearing pyrene at positions (a) 161, (b) 169, (c) 176, and (d) 181. Spectral measurements were taken as described in the legend of Figure 4. (C and D) Effect of 50% TFE (···) and 50% glycerol (---) on fluorescence emission features of pyrene-labeled (C) apoEC112S/V161C(1−299) and (D) apoEC112S/L181C(1−299). The spectra of these labeled variants in PBS are shown for comparison (—).

probe flexibility to excimer emission, and (iii) the organization of the linker segment of apoE in its tetrameric organization.

To accomplish these goals, it was important to have pairs of pyrene moieties located at defined distances apart from each other on a fairly long scaffold: for example, an α-helix approximately 25 Å long, wherein the repeating unit is a single turn that extends ∼5.4 Å along the helical axis, as depicted schematically in Figure 1A. We used sites facing away from the interior to allow equitable access and facile labeling with pyrene. In addition, it was essential to employ a molecule for which the high-resolution structure is available to develop a rational structure-guided approach. Helix 2 of apoE3(1−191) fulfilled most of the criteria: its high-resolution structure is known[24,25] and it is sufficiently long that it can bear two pyrenes up to ∼20 Å apart. All variants retained a helical structure. The variant with Cys residues at positions 59 and 66 alone showed a lower α-helical content; however, it did not affect the overall interpretation because the correlation between distance and pyrene excimer formation was noted in the presence of TFE, a helix-inducing solvent. A geometrical analysis of the X-ray structure of apoE (PDB entry 1NFN) using the HELANAL-Plus webserver software,[35] and using DSSP to identify helical segments,[36] identifies helix 2 (residues 55−78) as the only linear helix in this protein, quantitatively defined by a root-mean-square deviation of only 0.060 Å from an ideal linear helical axis, a maximal bend angle of only 5.8 ± 2.4° (including residues at the ends of the helix), and a radius of curvature of 167 Å. A similar analysis of the more recent NMR structure (PDB entry 2KC3) shows similar, albeit slightly higher, values for this helix. The chosen system of study thus serves as an ideal scaffold for the direct application and utility of pyrene excimer fluorescence in understanding structural information under physiologically relevant conditions, while also meeting the criteria specified above and limiting complications that might affect the interpretation of data.

Fluorescence emission spectra of pyrene-labeled double-Cys apoE variants revealed excimer formation to varying extents, with respect to the intensity of the first monomeric peak at 375 nm. Therefore, all spectra were normalized to the emission at 375 nm, which allows the direct comparison of the peak intensity at ∼460 nm. Throughout this work, the e/m ratio was used as a convenient way to compare different spectra, rather than the m/e ratio that is used conventionally by others and was used by us in previous studies.[19−21] Comparing the spectra of all the labeled double-Cys variants revealed an interesting observation: there was a distinct inverse correlation between the e/m ratio and the distance between two pyrene moieties. As predicted, the e/m value per se was relatively higher at higher concentrations (50 μg/mL), with values ranging from ∼3.0 to 1.4, and lower (from 2.6 to 1.2) at concentrations of 5−10 μg/mL. There was a minor contribution from intermolecular pyrene−pyrene interaction. Interestingly, the labeled variant with Cys residues at positions 59 and 66 had an e/m value that was lower than expected at lower concentrations; it is not known if this observation is position-specific or due to the behavior of two pyrenes at this distance or if the presence of pyrene at these locations affected the local secondary structure. Nevertheless, if the excimer we observed is due to intermolecular proximity alone, we would have seen a decrease not only in excimer intensity but also in the e/m ratio, corresponding to the dilution factor. However, we noted only a small decrease in e/m ratios, which was not congruent with the dilution factor. The persistent presence of the correlation even

dx.doi.org/10.1021/bi3005285 | *Biochemistry* 2012, 51, 6207−6219

in dilute samples is therefore indicative of intramolecular pyrene−pyrene interactions.

To confirm this observation, we followed the effect of TFE on the e/m ratio. TFE increases the level of α-helical elements by strengthening local interactions[37] and disrupting tertiary and quaternary structures by disrupting hydrophobic interactions.[10,38] A small decrease in excimer intensity was noted in the presence of TFE (Figure 6B); this is attributed to the loss of intermolecular interactions, a minor contribution. The red shift is attributed to interaction of the probes with the solvent and the relocation of the pyrenes to a more polar environment; the latter interpretation is supported by the decrease in the intensity of band III coupled to an increase in the intensity of a distinct band I peak. As reported above, there was a strong inverse correlation observed between the e/m ratio and separation distance in the presence of TFE (Figure 6D and Table 2).

Lastly, a progressive decrease was noted in the e/m ratio for each pair of labeled sites as the viscosity of the environment was increased. This suggests that in addition to separation distance, the mobility of the fluorophores plays a key role in the extent of excimer formation. The lifetime of pyrene fluorescence emission is long (50−90 ns), allowing observation of excimer fluorescence, with a higher mobility increasing and a lower mobility decreasing the probability of encounter between two pyrene moieties. A decrease in excimer yield corresponding to a decreased flexibility has been reported using pyrene-labeled tropomyosin: a higher excimer intensity was reported when the pyrene is located on a flexible segment.[39] When the flexibility was restricted because of interaction with actin or troponin, a decrease in excimer yield was noted.[40,41] Our results indicate that the excimer intensity can be attenuated by increasing the distance from 5 to 20 Å and by decreasing the probe mobility. It is important to keep in mind that the distances used in this study are between Cα and Cα atoms of residues prior to substitution, while the measured phenomenon occurs between pyrene rings attached via a maleimide functional group following Cys substitution. It is possible that the presence of the maleimide group may increase the mobility of the segment bearing the pyrene rings, allowing them to interact at distances of >5 Å.

While it is recognized that stacking interactions are an important factor for excimer formation, it is unclear why weak excimer formation was observed for pyrenes located 15−20 Å apart (E59C/K69C and E59C/A73C). This may be attributed to the inherent flexibility of the α-helical scaffold structure. Over the past decade, studies of protein secondary structure have dramatically improved our understanding of the α-helix. On short length scales, biological helices are quantitatively similar to a three-dimensional random walk, suggesting that such structures do not suffer significant entropic penalties upon the formation of structure.[42] On longer length scales, such as the 24-residue helix 2 studied here, helical peptides have been shown to exhibit transient local fluctuations away from the helical portion of the Ramachandran plot that effectively provide additional entropy to long helical segments.[43] With such fluctuations in mind, which may occur on the 1−10 ns time scale, "bending" or "breathing" modes within larger helical segments are expected. While tertiary interactions in the apoE helix bundle fold would expectedly add to the structural stability of helix 2, thereby decreasing the overall probability and magnitude of fluctuations in that helix, the time scales of such fluctuations remain well below the fluorescent lifetime of the pyrene excimer, thus suggesting that the excimer peak observed in the emission spectra at distances beyond 10 Å results primarily from helix flexibility. Accordingly, the use of glycerol to induce a reduction in mobility led to less prominent excimer peaks but did not affect the apparent inverse correlation between the e/m ratio and distance between pyrene pairs (Figure 6D and Table 2).

Our observations with pyrene-labeled apoE3T57C(1−191) support the validity of the observed correlation. The distance estimated from pyrene excimer formation (5.2 Å) agrees well with the distances in the X-ray and NMR structures (5.7 and 4.93 Å, respectively). However, factors such as the viscosity in the interior of the protein and differences in the orientation of the pyrene rings in the interior of the helix bundle may also affect excimer formation. In addition, C112 being "wedged" between helices 2 and 3 may further alter the orientation of the pyrene ring, thereby affecting excimer formation.

A recent study proposed the use of a pyrene maleimide derivative with a four-carbon methylene linker between the imide nitrogen of the maleimide and the pyrene ring[44] as a probe with a flexible spacer that will allow increased mobility. The authors suggest that the flexibility will facilitate placement of the probes at distances greater than the conventional distance of 5 Å; the putative use of this probe was demonstrated using thiol-modified 14 bp double-stranded oligonucleotides, where one thiol was located at the 5′ end of one strand and the other at the adjacent 3′ end of the complementary strand. Thus, in contrast to our design (of having two pyrenes along the helical axis), which provided more opportunities for pyrene−pyrene encounters and stacking interactions to occur, these authors' design of placing pyrenes at the ends of two interacting DNA strands limits the chances of stacking of the two pyrene rings, despite the mobility afforded by the flexible linker. In this context, an earlier study examining rabbit skeletal troponin C bearing pyrenes at positions 12 and 49,[45] which were found to be ∼33 Å apart by X-ray crystallography[46] (PDB entry 1TCF), displayed a weak excimer signal as observed herein, which was attributed to helix flexibility.

In a series of studies conducted by Kaback and colleagues, pyrene excimer fluorescence was employed to understand the organization, relative spatial disposition, and dynamics of the multiple transmembrane helices of *E. coli* lactose (lac) permease.[47−49] Lac permease is a membrane transport protein involved in the transduction of the free energy of an electrochemical proton gradient into substrate concentration gradient to drive the uphill accumulation of β-galactosides. It is a two-domain protein with N-terminal and C-terminal domains, each comprised of six transmembrane helices (numbered helices I−XII) that traverse the membrane in an antiparallel orientation. On the basis of the presence of excimer bands from pyrenes located on selected pairs of helices in recombinant lac permease (PDB entry 2CPF) reconstituted into proteoliposomes, the authors proposed that helix VIII (Glu269) is spatially proximal to helix X (His322) and helix IX (Arg302) is proximal to helix X (Glu325).[47,49] These observations were verified from the X-ray structure of this protein at 3.5 Å resolution in the absence and presence of bound ligand, a lactose homologue[50] (PDB entry 1PV6). The distance between the Cα pairs were found to be 10.2 Å (Glu269 and His322) and 9.9 Å (Arg302 and Glu325) based on the crystal structure.

Pyrene excimer fluorescence was also used to follow protein unfolding in human carbonic anhydrase II, which contains 10 β-

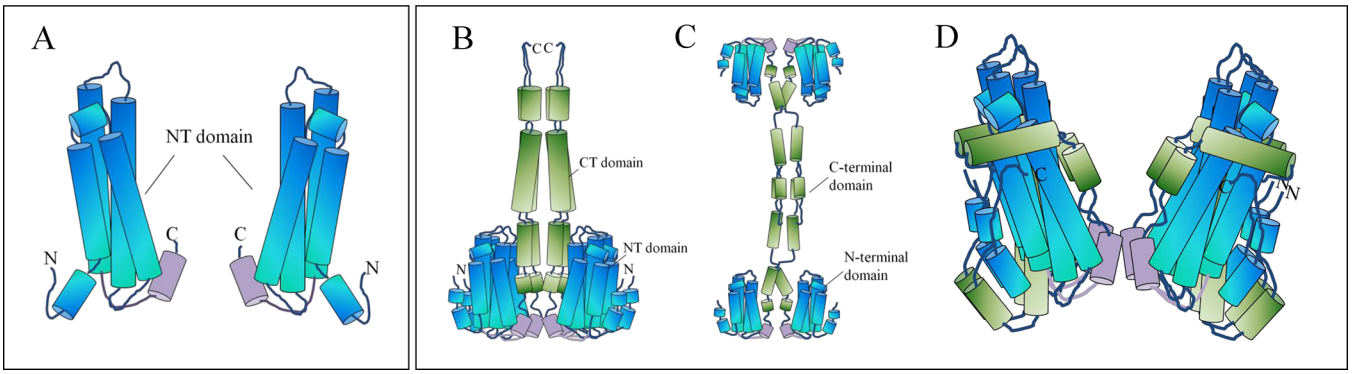

Figure 9. Proposed model for the tetrameric organization of apoE. Putative models of spatial organization of apoE3 are shown as schematic representations in the absence (A) and presence (B–D) of the CT domain. The segments probed in this study are colored purple. The CT domain is colored green and the NT domain blue. The dimeric apoE CT domains may be oriented parallel (B) or antiparallel (C). An alternative model of the tetrameric arrangement (D) reconciles with the proposed structure of monomeric apoE, assuming that the proposed monomeric structure is representative of the monomeric unit in the tetramer.

strands that form an open β-sheet.[51,52] The pyrenes were located on an engineered Cys at position 67 in β-strand 3 (N67C) and a single naturally occurring Cys at position 206 in β-strand 7.[53] Fluorescence emission spectra of pyrene-labeled N67C/C206 carbonic anhydrase revealed an e/m ratio of ~0.3; the X-ray structure at 2.0 Å resolution (PDB entry 1CA2) revealed a distance of 19.5 Å between Cα atoms of residues 67 and 206. Unlike the study presented here, the residues in carbonic anhydrase II were positioned across a sizable β-sheet, which are known to undergo much slower breathing modes than observed for protein α-helices.[54] Motions occurring on time scales beyond the lifetime of the excimer[11,55] may allow these labels to come into contact with each other but would thus be too slow to result in significant excimer emissions. Indeed, a strength of the approach presented here is the application of pyrene excimer emission to helical proteins, which could potentially be used to study not only the structural organization in such proteins but also the short time scale dynamics within such species.

In addition, pyrene excimer emission has also been used as a metric of the proximity between neighboring residues participating in intermolecular interactions. The segment from position 161 to 181 in isolated NT domain and full-length apoE3 was compared, using pyrene-labeled single-Cys proteins. In this case, intermolecular excimer formation was followed. The rationale behind comparing these two constructs was to test if the presence of the CT domain in the full-length protein altered the relative spatial proximity of the monomers in the tetrameric arrangement. It seems plausible that the self-association mediated by the CT domain juxtaposes the linker segment between the NT and CT domains from neighboring molecules in greater proximity in its native tetrameric configuration. Figure 9 shows some putative models of spatial organization of apoE3 as schematic representations in the absence and presence of the CT domain. In the absence of the CT domain (Figure 9A), the apoE3 NT domain is predominantly monomeric as shown by previous biochemical and biophysical studies and confirmed by us in this study. The low extent of excimer bands noted for pyrenes located between positions 161 and 181 possibly arises from some residual intermolecular interactions or from intramolecular interactions due to the proximity to aromatic residues in neighboring helices.

In the presence of the CT domain (green helices) (Figure 9B,C), apoE3 self-associates to form a tetramer, as suggested by previous biochemical and biophysical studies.[23,56−62] Previously, using the CT domain of pyrene-labeled apoE,[23] we noted that the entire CT domain of one apoE molecule associates with corresponding sites in a neighboring molecule to form a dimer, which likely dimerizes further in a parallel (Figure 9B) or antiparallel (Figure 9C) manner to mediate tetramerization.[23,57] The e/m ratios for pyrene located at positions 223, 255, and 277 were 3.3, 2.8, and 2.2, respectively. On the basis of the correlation plot from this study (Figure 6D), these e/m ratios are indicative of distances of 5, 8, and 10 Å, respectively. The progressive increase in distance suggests that the N-terminal ends of neighboring CT domains make closer intermolecular contacts relative to the C-terminal ends. This observation is consistent with our previous studies, which indicated that residues 210−264 are likely involved in a close intermolecular coiled-coil helix dimer configuration.[57] Studies from other groups suggest that residues 210−266 direct the relative lipoprotein binding preference of apoE.[63,64] Altogether, we envisage that the closer intermolecular proximity in this segment serves to protect the lipoprotein binding sites by shielding the hydrophobic face of the amphipathic helices from the aqueous environment in lipid-free apoE. Further, it is likely that the terminal segment (residues 266−299) is splayed, possibly forming an intermolecular four-helix bundle. This segment may be involved in initiating lipid binding of apoE. Lastly, pyrene located at position 209 yielded an e/m ratio of 0.5, indicative of distances of >22 Å. This is consistent with data from this study in which pyrene located at various sites along the linker segment (toward the N-terminal side of position 209) was 20−30 Å from corresponding sites on neighboring molecules.

A recent report on the NMR structure of a monomeric form of apoE bearing several critical mutations to prevent self-association[65] indicates three domains: an NT domain (residues 1−167), a hinge domain (residues 168−205), and a CT domain (residues 206−299); the hinge domain bears helices H1 (residues 168−180) and H2 (residues 190−199), while the CT domain bears helices C1−C3, corresponding to residues 210−223, 236−266, and 271−276, respectively. While it is not known if the structure of the forced monomer recapitulates the structure of the monomeric unit in the context of the tetramer, the CT domain is separated from the hinge domain by the NT

dx.doi.org/10.1021/bi3005285 | *Biochemistry* 2012, 51, 6207−6219

domain in the three-dimensional structure of the monomer. The study presented here probes the region corresponding to hinge H1 in the NMR structure, but in the context of the tetrameric protein. Self-association of apoE appears to juxtapose this segment to an average distance of ~10 Å from each other. While we cannot completely exclude the enhancing effect of the presence of pyrene in driving the juxtaposition of this segment, we propose that it is the intrinsic tendency of the α-helix encompassed by residues 168−180 to make extensive helix−helix contact that makes the pyrene rings spatially proximal.

In an attempt to explain the observations presented here with pyrene excimer fluorescence in light of the proposed structure of monomeric apoE,[65] we consider a putative model (Figure 9D) of tetrameric apoE, with the linker segments from neighboring molecules proximal to each other. Our previous cross-linking and pyrene excimer fluorescence analyses with apoE(201−299)[23,57] juxtaposed positions 223, 255, and 277 from neighboring molecules, observations that are not consistent with this model. Further studies are needed to understand the organization of the CT domain in the context of the full-length tetrameric protein, which is particularly relevant in the context of apoE4, an isoform considered a risk factor for Alzheimer's disease. In contrast to apoE3 that bears a Cys at position 112, apoE4 bears an Arg. A salt bridge between R61 in the NT domain and E255 in the CT domain of apoE4[63,66] has been proposed to juxtapose the two domains. A moderate excimer fluorescence was noted between pyrene-labeled R61C and E255C,[34] which suggested spatial proximity between these sites. Taken together with other biochemical and biophysical properties of apoE4, this domain interaction is believed to play a significant role in the unique and anomalous behavior of this isoform.[67] Without a high-resolution structure of apoE4 in its native configuration, the molecular basis for this predisposition is not known, and more studies are needed to understand the structure−function relationships in apoE.

AUTHOR INFORMATION

Corresponding Author

*Department of Chemistry and Biochemistry, 1250 Bellflower Blvd., California State University Long Beach, Long Beach, CA 90840. Telephone: (562) 985-4953. Fax: (562) 985-8557. E-mail: vas.narayanaswami@csulb.edu.

Funding

This work was funded by the Tobacco Related Disease Research Program (TRDRP 17RT-0165), National Institutes of Health Grant HL096365, a CSUPERB Faculty Development Grant (V.N.), and the Michael Monahan award (G.K.B.).

Notes

The authors declare no competing financial interest.

ABBREVIATIONS

apoE, apolipoprotein E; CD, circular dichroism; CT, C-terminal; DTT, dithiothreitol; *e*/*m*, excimer/monomer; GdnHCl, guanidine hydrochloride; NPM, *N*-(1-pyrene)-maleimide; NT, N-terminal; PBS, phosphate-buffered saline [10 mM sodium phosphate (pH 7.4) and 150 mM NaCl]; PDB, Protein Data Bank; TFE, 2,2,2-trifluoroethanol; WT, wild type.

REFERENCES

(1) Benecky, M. J., Kolvenbach, C. G., Wine, R. W., DiOrio, J. P., and Mosesson, M. W. (1990) Human plasma fibronectin structure probed by steady-state fluorescence polarization: Evidence for a rigid oblate structure. *Biochemistry 29*, 3082−3091.

(2) Benecky, M. J., Wine, R. W., Kolvenbach, C. G., and Mosesson, M. W. (1991) Ionic-strength- and pH-dependent conformational states of human plasma fibronectin. *Biochemistry 30*, 4298−4306.

(3) Zolese, G., Rabini, R. A., Fumelli, P., Staffolani, R., Curatola, A., Kvasnicka, P., Kotyk, A., Cester, N., and Mazzanti, L. (1997) Modifications induced by insulin-dependent diabetes mellitus on human placental Na^+/K^+-adenosine triphosphatase. *J. Lab. Clin. Med. 130*, 374−380.

(4) Linnertz, H., Miksik, I., Kvasnicka, P., Bertoli, E., Mazzanti, L., Schoner, W., and Amler, E. (1998) Binding of pyrene isothiocyanate to the E1ATP site makes the H4-H5 cytoplasmic loop of Na^+/K^+-ATPase rigid. *Eur. J. Biochem. 251*, 522−527.

(5) Haugland, R. P., Spence, M. T. Z., Johnson, I. D., and Basey, A. (2005) *The handbook: A guide to fluorescent probes and labeling technologies*, 10th ed., Molecular Probes, Eugene, OR.

(6) Karpovich, D. S., and Blanchard, G. J. (1995) Relating the polarity-dependent fluorescence response of pyrene to vibronic coupling. Achieving a fundamental understanding of the *py* polarity scale. *J. Phys. Chem. 99*, 3951−3958.

(7) Peter Geigle, K., Wolf, J., and Hohlneicher, G. (1997) Franck-Condon/Herzberg-Teller interferences in the 1Lb transitions of pyrene and chrysene. *J. Photochem. Photobiol., A 105*, 183−187.

(8) Hara, K., and Ware, W. (1980) Influence of solvent perturbation on the radiative transition probability from the 1B1u state of pyrene. *Chem. Phys. 51*, 61−68.

(9) Nakajima, A. (1982) Intensity enhancement induced by solute-solvent interaction between pyrene and polar solvents. *Spectrochim. Acta 38A*, 693−695.

(10) Kalyanasundaram, K., and Thomas, J. K. (1977) Environmental effects on vibronic band intensities in pyrene monomer fluorescence and their application in studies of micellar systems. *J. Am. Chem. Soc. 99*, 2039−2044.

(11) Lehrer, S. S. (1995) Pyrene excimer fluorescence as a probe of protein conformational change. *Subcell. Biochem. 24*, 115−132.

(12) Birks, J. B. (1970) *Photophysics of aromatic molecules*, Wiley-Interscience, New York.

(13) Somerharju, P. (2002) Pyrene-labeled lipids as tools in membrane biophysics and cell biology. *Chem. Phys. Lipids 116*, 57−74.

(14) Birks, J. B. (1968) Triplet-triplet interaction of aromatic molecules in solution. *Chem. Phys. Lett. 2*, 417−419.

(15) Winnick, F. M. (1993) Photophysics of preassociated pyrenes in aqueous polymer solutions and in other organized media. *Chem. Rev. 93*, 587−614.

(16) Newcomb, L. F., and Gellman, S. H. (1994) Aromatic Stacking Interactions in Aqueous Solution: Evidence That neither Classical Hydrophobic Effects nor Dispersion Forces Are Important. *J. Am. Chem. Soc. 116*, 4993−4994.

(17) Bains, G., Patel, A. B., and Narayanaswami, V. (2011) Pyrene: A probe to study protein conformation and conformational changes. *Molecules 16*, 7909−7935.

(18) Narayanaswami, V., and Ryan, R. O. (2000) Molecular basis of exchangeable apolipoprotein function. *Biochim. Biophys. Acta 1483*, 15−36.

(19) Sahoo, D., Weers, P. M., Ryan, R. O., and Narayanaswami, V. (2002) Lipid-triggered conformational switch of apolipophorin III helix bundle to an extended helix organization. *J. Mol. Biol. 321*, 201−214.

(20) Sahoo, D., Narayanaswami, V., Kay, C. M., and Ryan, R. O. (2000) Pyrene excimer fluorescence: A spatially sensitive probe to monitor lipid-induced helical rearrangement of apolipophorin III. *Biochemistry 39*, 6594−6601.

(21) Sahoo, D., Narayanaswami, V., Kay, C. M., and Ryan, R. O. (1998) Fluorescence studies of exchangeable apolipoprotein-lipid

interactions. Superficial association of apolipophorin III with lipoprotein surfaces. *J. Biol. Chem. 273*, 1403−1408.
(22) Wang, J., Sykes, B. D., and Ryan, R. O. (2002) Structural basis for the conformational adaptability of apolipophorin III, a helix-bundle exchangeable apolipoprotein. *Proc. Natl. Acad. Sci. U.S.A. 99*, 1188−1193.
(23) Patel, A. B., Khumsupan, P., and Narayanaswami, V. (2010) Pyrene fluorescence analysis offers new insights into the conformation of the lipoprotein-binding domain of human apolipoprotein E. *Biochemistry 49*, 1766−1775.
(24) Wilson, C., Wardell, M. R., Weisgraber, K. H., Mahley, R. W., and Agard, D. A. (1991) Three-dimensional structure of the LDL receptor-binding domain of human apolipoprotein E. *Science 252*, 1817−1822.
(25) Sivashanmugam, A., and Wang, J. (2009) A unified scheme for initiation and conformational adaptation of human apolipoprotein E N-terminal domain upon lipoprotein binding and for receptor binding activity. *J. Biol. Chem. 284*, 14657−14666.
(26) Gupta, V., Narayanaswami, V., Budamagunta, M. S., Yamamato, T., Voss, J. C., and Ryan, R. O. (2006) Lipid-induced extension of apolipoprotein E helix 4 correlates with low density lipoprotein receptor binding ability. *J. Biol. Chem. 281*, 39294−39299.
(27) Morrow, J. A., Segall, M. L., Lund-Katz, S., Phillips, M. C., Knapp, M., Rupp, B., and Weisgraber, K. H. (2000) Differences in stability among the human apolipoprotein E isoforms determined by the amino-terminal domain. *Biochemistry 39*, 11657−11666.
(28) Redmond, K. A., Murphy, C., Narayanaswami, V., Kiss, R. S., Hauser, P., Guigard, E., Kay, C. M., and Ryan, R. O. (2006) Replacement of helix 1′ enhances the lipid binding activity of apoE3 N-terminal domain. *FEBS J. 273*, 558−567.
(29) De Pauw, M., Vanloo, B., Weisgraber, K., and Rosseneu, M. (1995) Comparison of lipid-binding and lecithin:cholesterol acyltransferase activation of the amino- and carboxyl-terminal domains of human apolipoprotein E3. *Biochemistry 34*, 10953−10966.
(30) Zhao, M., Zen, K. C., Hubbell, W. L., and Kaback, H. R. (1999) Proximity between Glu126 and Arg144 in the lactose permease of *Escherichia coli*. *Biochemistry 38*, 7407−7412.
(31) Liou, Y. M., and Chen, M. W. (2003) Calcium-dependent protein-protein interactions induce changes in proximity relationships of Cys48 and Cys64 in chicken skeletal troponin I. *Eur. J. Biochem. 270*, 3092−3100.
(32) Santra, M. K., Dasgupta, D., and Panda, D. (2006) Pyrene excimer fluorescence of yeast alcohol dehydrogenase: A sensitive probe to investigate ligand binding and unfolding pathway of the enzyme. *Photochem. Photobiol. 82*, 480−486.
(33) West, J. M., Tsuruta, H., and Kantrowitz, E. R. (2004) A fluorescent probe-labeled *Escherichia coli* aspartate transcarbamoylase that monitors the allosteric conformational state. *J. Biol. Chem. 279*, 945−951.
(34) Drury, J., and Narayanaswami, V. (2005) Examination of lipid-bound conformation of apolipoprotein E4 by pyrene excimer fluorescence. *J. Biol. Chem. 280*, 14605−14610.
(35) Bansal, M., Kumar, S., and Velavan, R. (2000) HELANAL: A program to characterize helix geometry in proteins. *J. Biomol. Struct. Dyn. 17*, 811−819.
(36) Kabsch, W., and Sander, C. (1983) Dictionary of protein secondary structure: Pattern recognition of hydrogen-bonded and geometrical features. *Biopolymers 22*, 2577−2637.
(37) Thomas, P. D., and Dill, K. A. (1993) Local and nonlocal interactions in globular proteins and mechanisms of alcohol denaturation. *Protein Sci. 2*, 2050−2065.
(38) Lau, S. Y., Taneja, A. K., and Hodges, R. S. (1984) Synthesis of a model protein of defined secondary and quaternary structure. Effect of chain length on the stabilization and formation of two-stranded α-helical coiled-coils. *J. Biol. Chem. 259*, 13253−13261.
(39) Burtnick, L. D., Stewart, D. I., Clark, I. D., and Smillie, L. B. (1986) Excimer fluorescence of equine platelet tropomyosin labeled with N-(1-pyrenyl)iodoacetamide. *Biochemistry 25*, 3875−3880.
(40) Ishii, Y., and Lehrer, S. S. (1985) Fluorescence studies of the conformation of pyrene-labeled tropomyosin: Effects of F-actin and myosin subfragment 1. *Biochemistry 24*, 6631−6638.
(41) Ishii, Y., and Lehrer, S. S. (1991) Two-site attachment of troponin to pyrene-labeled tropomyosin. *J. Biol. Chem. 266*, 6894−6903.
(42) Zagrovic, B., and Pande, V. S. (2003) Structural correspondence between the α-helix and the random-flight chain resolves how unfolded proteins can have native-like properties. *Nat. Struct. Biol. 10*, 955−961.
(43) Sorin, E. J., and Pande, V. S. (2005) Exploring the helix-coil transition via all-atom equilibrium ensemble simulations. *Biophys. J. 88*, 2472−2493.
(44) Niwayama, S., Kassar, A. S., Zhao, T., Sutton, R. B., and Altenberg, G. A. (2011) A pyrene maleimide with a flexible linker for sampling of longer inter-thiol distances by excimer formation. *PLoS One 6*, e26691.
(45) Wang, Z., Gergely, J., and Tao, T. (1992) Characterization of the Ca^{2+}-triggered conformational transition in troponin C. *Proc. Natl. Acad. Sci. U.S.A. 89*, 11814−11817.
(46) Soman, J., Tao, T., and Phillips, G. N., Jr. (1999) Conformational variation of calcium-bound troponin C. *Proteins 37*, 510−511.
(47) Jung, K., Jung, H., Wu, J., Prive, G. G., and Kaback, H. R. (1993) Use of site-directed fluorescence labeling to study proximity relationships in the lactose permease of *Escherichia coli*. *Biochemistry 32*, 12273−12278.
(48) Jung, K., Jung, H., and Kaback, H. R. (1994) Dynamics of lactose permease of *Escherichia coli* determined by site-directed fluorescence labeling. *Biochemistry 33*, 3980−3985.
(49) Kaback, H. R., Frillingos, S., Jung, H., Jung, K., Prive, G. G., Ujwal, M. L., Weitzman, C., Wu, J., and Zen, K. (1994) The lactose permease meets Frankenstein. *J. Exp. Biol. 196*, 183−195.
(50) Abramson, J., Smirnova, I., Kasho, V., Verner, G., Kaback, H. R., and Iwata, S. (2003) Structure and mechanism of the lactose permease of *Escherichia coli*. *Science 301*, 610−615.
(51) Hakansson, K., Carlsson, M., Svensson, L. A., and Liljas, A. (1992) Structure of native and apo carbonic anhydrase II and structure of some of its anion-ligand complexes. *J. Mol. Biol. 227*, 1192−1204.
(52) Eriksson, A. E., Jones, T. A., and Liljas, A. (1988) Refined structure of human carbonic anhydrase II at 2.0 Å resolution. *Proteins 4*, 274−282.
(53) Hammarstrom, P., Kalman, B., Jonsson, B. H., and Carlsson, U. (1997) Pyrene excimer fluorescence as a proximity probe for investigation of residual structure in the unfolded state of human carbonic anhydrase II. *FEBS Lett. 420*, 63−68.
(54) Akke, M., Liu, J., Cavanagh, J., Erickson, H. P., and Palmer, A. G., III (1998) Pervasive conformational fluctuations on microsecond time scales in a fibronectin type III domain. *Nat. Struct. Biol. 5*, 55−59.
(55) Conlon, P., Yang, C. J., Wu, Y., Chen, Y., Martinez, K., Kim, Y., Stevens, N., Marti, A. A., Jockusch, S., Turro, N. J., and Tan, W. (2008) Pyrene excimer signaling molecular beacons for probing nucleic acids. *J. Am. Chem. Soc. 130*, 336−342.
(56) Westerlund, J. A., and Weisgraber, K. H. (1993) Discrete carboxyl-terminal segments of apolipoprotein E mediate lipoprotein association and protein oligomerization. *J. Biol. Chem. 268*, 15745−15750.
(57) Choy, N., Raussens, V., and Narayanaswami, V. (2003) Inter-molecular coiled-coil formation in human apolipoprotein E C-terminal domain. *J. Mol. Biol. 334*, 527−539.
(58) Garai, K., and Frieden, C. (2010) The association-dissociation behavior of the ApoE proteins: Kinetic and equilibrium studies. *Biochemistry 49*, 9533−9541.
(59) Aggerbeck, L. P., Wetterau, J. R., Weisgraber, K. H., Wu, C. S., and Lindgren, F. T. (1988) Human apolipoprotein E3 in aqueous solution. II. Properties of the amino- and carboxyl-terminal domains. *J. Biol. Chem. 263*, 6249−6258.
(60) Wetterau, J. R., Aggerbeck, L. P., Rall, S. C., and Weisgraber, K. H. (1988) Human apolipoprotein E3 in aqueous solution. I. Evidence for two structural domains. *J. Biol. Chem. 263*, 6240−6248.

(61) Sakamoto, T., Tanaka, M., Vedhachalam, C., Nickel, M., Nguyen, D., Dhanasekaran, P., Phillips, M. C., Lund-Katz, S., and Saito, H. (2008) Contributions of the carboxyl-terminal helical segment to the self-association and lipoprotein preferences of human apolipoprotein E3 and E4 isoforms. *Biochemistry 47*, 2968−2977.
(62) Saito, H., Lund-Katz, S., and Phillips, M. C. (2004) Contributions of domain structure and lipid interaction to the functionality of exchangeable human apolipoproteins. *Prog. Lipid Res. 43*, 350−380.
(63) Dong, L. M., Wilson, C., Wardell, M. R., Simmons, T., Mahley, R. W., Weisgraber, K. H., and Agard, D. A. (1994) Human apolipoprotein E. Role of arginine 61 in mediating the lipoprotein preferences of the E3 and E4 isoforms. *J. Biol. Chem. 269*, 22358−22365.
(64) Weisgraber, K. H., and Mahley, R. W. (1996) Human apolipoprotein E: The Alzheimer's disease connection. *FASEB J. 10*, 1485−1494.
(65) Chen, J., Li, Q., and Wang, J. (2011) Topology of human apolipoprotein E3 uniquely regulates its diverse biological functions. *Proc. Natl. Acad. Sci. U.S.A. 108*, 14813−14818.
(66) Dong, L. M., and Weisgraber, K. H. (1996) Human apolipoprotein E4 domain interaction. Arginine 61 and glutamic acid 255 interact to direct the preference for very low density lipoproteins. *J. Biol. Chem. 271*, 19053−19057.
(67) Hatters, D. M., Peters-Libeu, C. A., and Weisgraber, K. H. (2006) Apolipoprotein E structure: Insights into function. *Trends Biochem. Sci. 31*, 445−454.